Integrated design of flight control surfaces and laws for new aircraft configurations

Y. Denieul * **J. Bordeneuve-Guibé** ** **D. Alazard** *** **C. Toussaint** **** **G. Taquin** †

* *PhD Student, University of Toulouse, ISAE-SUPAERO, 10, Av. Edouard Belin, 31055 Toulouse FRANCE*
** *Associated Professor, University of Toulouse, ISAE-SUPAERO, 10, Av. Edouard Belin, 31055 Toulouse FRANCE.*
*** *Professor, University of Toulouse, ISAE-SUPAERO, 10, Av. Edouard Belin, 31055 Toulouse FRANCE.*
**** *Research Engineer, ONERA, 2, Av. Edouard Belin, 31055 Toulouse FRANCE.*
† *Handling Qualities Expert, Airbus Opérations SAS, 316 route de Bayonne, 31060 Toulouse FRANCE.*

Abstract: Control architecture sizing is a main challenge for new aircraft design like blended wing-body design. This aircraft configuration typically features redundant elevons located at the trailing edge of the wing, acting simultaneously on pitch and roll axes. The problem of integrated design of control surface sizes and flight control laws for an unstable blended wing-body aircraft is addressed here. Latest tools for H_∞ non-smooth optimization of structured controllers are used to optimize in a single step the gains for both longitudinal and lateral control laws, and a control allocation module, while minimizing control surfaces total span. Following constraints are ensured: maximal deflection angles and rates for 1) pilot longitudinal pull-up 2) pilot bank angle order and 3) longitudinal turbulence. Using this coupled approach, significant gains in terms of outer elevons span compared to the initial layout are demonstrated, while closed-loop handling qualities constraints are guaranteed.

Keywords: Integrated design, Flight Control Law, Aircraft, H_∞ control, Dynamics, BWB

1. INTRODUCTION

Among other disruptive aircraft configurations, the Blended Wing-Body (BWB) was identified for years as a promising candidate for the future of civil aviation Liebeck (2004). The rationale for this game-changing configuration is as follows: instead of considering separate geometrical components for each basic function of an aircraft, namely *Lift, Transport, Control* and *Propulsion*, the BWB gathers the three former functions into a single lifting surface. As a consequence of this functions merging, an overall improved efficiency is expected, implying significant gains in terms of fuel consumption Martínez-Val and Pérez (2005); Liebeck (2004); Qin et al. (2004); Bolsunovsky et al. (2001). This paper focuses on an Airbus long-range BWB configuration.

Major challenges yet to be solved before a potential entry into service include control-related issues Roman et al. (2000). These issues first originate from the nature of the control devices used for this configuration: the BWB is controlled with multi-control surfaces, also named elevons, usually spanning the whole trailing-edge and acting as pitch and roll devices. Among challenges implied by this technology, new handling qualities criteria are required in order to take into account the combined authority of control surfaces on longitudinal and lateral axes. This was already addressed in a previous work Saucez and Boiffier (2012).

Then concerning control surfaces area sizing, two phenomena have a combined detrimental effect both on actuators mass and power consumption Roskam (1985). On the one hand, trailing edge elevons induce high aerodynamic hinge moments due to their large area. On the other hand, high deflection rates result from the longitudinal stabilization of an unstable configuration. Indeed the Airbus BWB features a negative static margin, specially at low speed (see section 2.2), i.e. an unstable short-period mode. For that reason it requires a permanent Stability Augmentation System (SAS) in order to guarantee adequate safety and handling qualities. However it was shown in a previous study Denieul et al. (2015a) that the more unstable an aircraft, the faster its control surfaces need to move in order to maintain the equilibrium under disturbance. This effect is even increased on the BWB, for elevons lack longitudinal lever arm with respect to center of gravity (CG). During preliminary design phase, control surfaces pitch efficiency should then be sought to be maximized, for instance by increasing control surfaces area as much as possible, which is conflicting with previously mentioned requirement on hinge moments limitation.

Both large hinge moments and high deflection rates have a direct impact on FCS sizing and secondary power con-

⋆ This work is supported by ANRT and AIRBUS.

10.1016/j.ifacol.2017.08.2085

sumption. Indeed as stated by Garmendia et al. Garmendia et al. (2014), secondary power for FCS P_{FCS} may be evaluated in a preliminary way by the equation (1):

$$P_{FCS} = \sum_{i=1}^{n_{controls}} HM_i^{max}.\dot{\theta}_i^{max} \quad (1)$$

where HM_i^{max} and $\dot{\theta}_i^{max}$ are the maximum hinge moment and maximum deflection rate of the i-th control surface respectively, and $n_{controls}$ is the number of control surfaces.

At preliminary design phase, when actuators sizing is not yet frozen, deflection rate is a direct consequence of control laws design. Also the traditional way of sizing conventional control surfaces considers simplified open-loop handling qualities criteria, such as roll rate target for the ailerons or pitch rate target for the elevator. Such an approach is no more valid for BWB control surface sizing due to the natural pitch instability: control surface areas may be largely sized by stabilization requirements, so sizing requires considering control laws at the early design phase. Control laws design in turn depends on control surfaces effectiveness. This coupled problem is known in control community as *plant-controller optimization* or *integrated design and control*. Classical way of handling this problem involves an iterative approach: effectors are sized based on engineering rules, then a control law is designed. If requirements are not met, then the sizing is changed based on the existing control law, and so on. However it is proved Fathy et al. (2001) that beyond being time-consuming, this approach may miss the optimum because of the tightly coupled nature of the problem. Consequently, several approaches are seeking solving these combined problems in a single step. "Plant-controller optimization" was studied in a variety of domains, such as chemistry Ricardez-Sandoval et al. (2009), autonomous underwater vehicles Silvestre et al. (1998) and astronautics Alazard et al. (2013); Denieul et al. (2015b,a).

In the field of aeronautics two complementary approaches were studied. The first method considers integrating a stability and control module into a multidisciplinary optimization (MDO) process Perez et al. (2006). A second more control-oriented approach takes advantage of optimization tools developped for controllers design in order to simultaneously optimize a controller and some meaningful physical parameters. Niewoehner and Kaminer (1996) optimized in a single loop a longitudinal controller and elevator control surface using linear matrix inequalities (LMI) framework. More recently, nonsmooth optimization methods enabling structured linear varying paremeters (LPV) controllers were applied to the longitudinal integrated design and control problem Lhachemi et al. (2015).

We propose to extend this approach to longitudinal / lateral integrated design and control of a BWB by optimizing together a three-axes control laws and control surfaces total span, using nonsmooth optimization techniques for fixed structure controllers. The main contribution of this paper is to optimize in a single step the control surfaces span, the control allocation module, and flight control laws, in order to guarantee longitudinal and lateral handling qualities constraints with a minimum control surfaces size.

This paper is organized as follows: in section 2 the flight dynamics models are presented. Then section 3 introduces the strategy for parameterizing the elevons total span, and obtaining a parametrized state-space representation suitable for optimization. The integrated design and control problem of computing structured longitudinal / lateral control laws gains together with optimal elevons size is presented in section 4, and results are discussed in section 5.

2. AIRCRAFT FLIGHT DYNAMICS AND CONTROL

In this section the models used in sections 3 and 4 for design, control and simulation are described. The configuration studied in this paper is a long-range BWB whose planform results from optimization studies on high-speed performance with constraints on low-speed pitching moment Meheut et al. (2012). The focus of this work is the sizing of control surfaces; thus, the planform is considered constant. The planform and initial control surfaces layout are visible on Figure 2(a).

2.1 Linear Model of Flight Dynamics Equations

In order to perform control laws synthesis and linear analysis, Flight Dynamics equations are linearized around equilibrium flight points. These initial equilibria are computed for the following conditions: zero flight path angle, sideslip and bank angle. At a given flight operating conditions in terms of mass (m), Mach number (M) and altitude (H), the 3-axis model state-space representation reads:

$$\dot{X} = AX + BU + B_w w_z \quad (2)$$

$$Y = CX + DU + D_w w_z \quad (3)$$

where $X = [\delta V \ \delta\alpha \ q \ \delta\theta \ \beta \ p \ r \ \phi]^T$ is the state vector composed of $\delta V = V - V_e$ the relative airspeed with respect to the equilibrium speed, $\delta\alpha = \alpha - \alpha_e$ and $\delta\theta = \theta - \theta_e$ relative angle of attack and pitch attitude with respect to the equilibrium respectively, sideslip β and p, q, r rotation rates of the aircraft with respect to the earth reference frame in roll, pitch and yaw respectively. $U = [\Delta\delta m^T, \ \delta n]^T$ is the control vector composed of $\Delta\delta m = [\Delta\delta m_i]^T, \ i = 1 \dots 10$ with $\Delta\delta m_i = \delta m_i - \delta m_e$ the relative deflection of the $i-th$ elevon control surface with respect to the equilibrium position. Each of the 10 elevons is actuated independently, through a control allocation strategy presented in 4.2. Elevons layout shown in Figure 2(a) is ordered in the control vector as follows: $\delta m_{i,i=1\dots10} = [LDQ1 \dots LDQ5, RDQ1 \dots RDQ5]$. Control vector also contains rudder deflection δn. While two rudders are visible on the configuration of Figure 2(a) (LDR and RDR), it was chosen for sake of clarity to group them as a single control with twice the efficiency of one rudder; the aim of our study is indeed not to size vertical surfaces but only elevons. The output vector $Y = [N_z, \ q, \ \beta, \ p, \ r, \ \phi]^T$ is composed of the vertical load factor Nz and the measured state variables. Finally turbulence effect is included as a vertical velocity w_z expressed in the earth reference frame, under the assumption that it acts as an increment of angle of attack. The model used for turbulence is described in section 2.3.

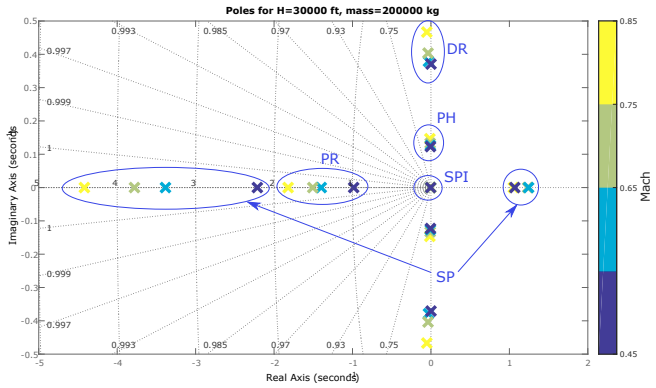

Fig. 1. Poles of aircraft dynamics for backward CG.

2.2 Modes Analysis

For a given Aircraft configuration, the coefficients of state-space matrices (Eq. (2) and (3) depends on the flight conditions (m, M and H). The modes of the eight-states aircraft dynamics presented in Eq. (2) are depicted in Figure 1. For sake of clarity poles are shown only for one mass and altitude, with Mach number varying between 0.45 to 0.85. The main point to retain from Figure 1 is the strong instability of the short-period (SP) oscillation and a poorly damped dutch roll mode (DR).

2.3 Turbulence Model

A Dryden continuous turbulence model is used for simulating vertical continuous turbulence w_z. A band-limited white noise e_w is passed through a forming filter approximating the Dryden velocity spectra. The transfer function has the following expression from Standard (1990):

$$H_{w_z}(s) = \frac{w_z}{e_w}(s) = \sigma_z \sqrt{\frac{2L_z}{\pi V}} \frac{1 + \frac{\sqrt{3}L_z}{V}s}{(1 + \frac{L_z}{V}s)^2} \tag{4}$$

where V is the aircraft airspeed, L_z is the vertical turbulence scale length that was set to 500 m and S is te reference area.

2.4 Actuators Model

A second-order actuators model accounting for their bandwidth and damping is used:

$$\frac{y_{act}}{u_{act}} = \frac{\omega_0^2}{s^2 + 2\xi\omega_0 s + \omega_0^2} \tag{5}$$

A single bandwidth and damping of respectively $\omega_0 = 1.4Hz$ and $\xi = 0.8$ was used. Previous studies considered allocating different bandwidth for all control surfaces Denieul et al. (2015a,b), however this is out of the scope of present paper. A 100 ms delay (approximated by a second-order Padé filter) accounting for sensors, computers and data processing is included in the control law synthesis and simulation. Actuators and delay are visible on control law structure of Figure 5.

3. PARAMETRIC REPRESENTATION OF CONTROL SURFACES SPAN VARIATION

In this section a process for obtaining a continuous approximation of control surfaces efficiencies for varying outer elevons span is presented. This part aims at obtaining a continuously parametrized state-space representation, so that the continuous optimizer presented in section 4 may use the continuous variable representing elevons size as an optimization variable.

3.1 Geometric Parametrization of Control Surfaces Span

Outer elevons total span is chosen as a plant Figure-of-merit to be minimized. More precisely a variable η representing the ratio of outer elevons total span compared to the initial control surfaces span is introduced. On Figure 2(a) initial elevons layout, corresponding to parameter value $\eta = 1$ is presented. This initial layout features five control surfaces on each side of the wing spanning the whole trailing edge, except a gap between elevon 1 and 2 for engine pylon integration – elevons are numbered from inboard to outboard. Elevons relative chord is limited in $x-$wise position by cabin integration for elevon 1, and by rear spar for elevons 2 to 5. So it was decided: (i) elevon 1 is constant, (ii) relative chord and span are constant for elevons 2 to 5 (split equally on the outer wing), (iii) the number of elevons is constant. Elevons number is mostly a failure cases problem that is out of scope of our study.

It is then clear that $0 \leq \eta \leq 1$, $\eta = 1$ corresponding to initial elevons layout and $\eta = 0$ corresponding to the lack of any control surface on the outer wing. Examples of layouts for $\eta = 0.8$ and $\eta = 0.4$ are presented on Figures 2(b) and 2(c) respectively.

3.2 Computation of Aerodynamic Models as a function of the Control Surface Span η

For a given flight condition (m, M and H), the coefficients of state-space matrices (Eq. (2) and (3) depends on the Aircraft configuration parameter (reduced to η in this study) through the aerodynamic coefficients. Since the plan-form and the airfoils are kept constant for all configurations, the varying coefficients are the control surface aerodynamic coefficients which impact only the control effectiveness matrix: $B = B(\eta)$.

Computation of aerodynamic model for different parameter values of η is described in this section. The goal is to obtain state-space representations continuously parametrized by elevon span parameter η. Process to obtain such a continuous approximation is presented on Figure 3. A first step is to compute calibrated aerodynamic models for discrete values of η, namely for values between 0.1 and 1 with steps of 0.1. For that purpose the Athena Vortex Lattice (AVL) software Drela and Youngren (2006) was used together with calibration factors coming from the supposedly known aerodynamic coefficients of the initial BWB design. This method combines the advantages of fast data generation through light CFD computation, and far better accuracy than AVL direct output through accurate knowledge on a reference configuration. It provides a set of control effectiveness matrices B_{η_k} for N sampled values η_k of η: $\eta_{k,k=1:N} = [0.1, \cdots, 1]$.

Once aerodynamic coefficients are computed and calibrated for discretized values of η, the final step consists in obtaining an approximation of the function $B(\eta)$. For that purpose it was chosen to work with the Linear Fractional

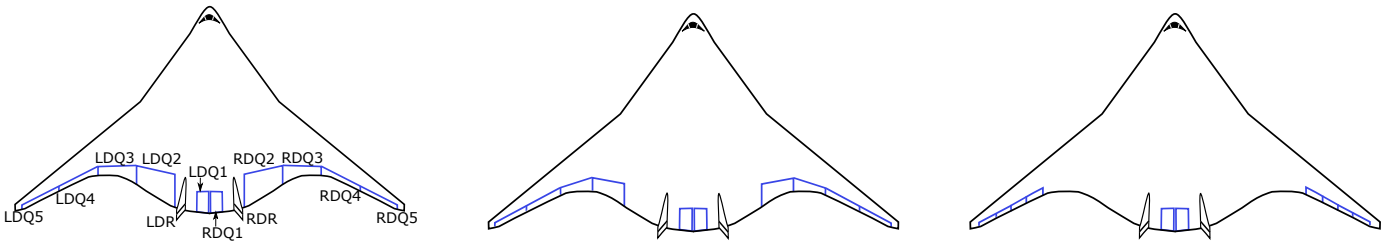

(a) $\eta = 1$ (b) $\eta = 0.8$ (c) $\eta = 0.4$

Fig. 2. Elevons size for different values of parameter η.

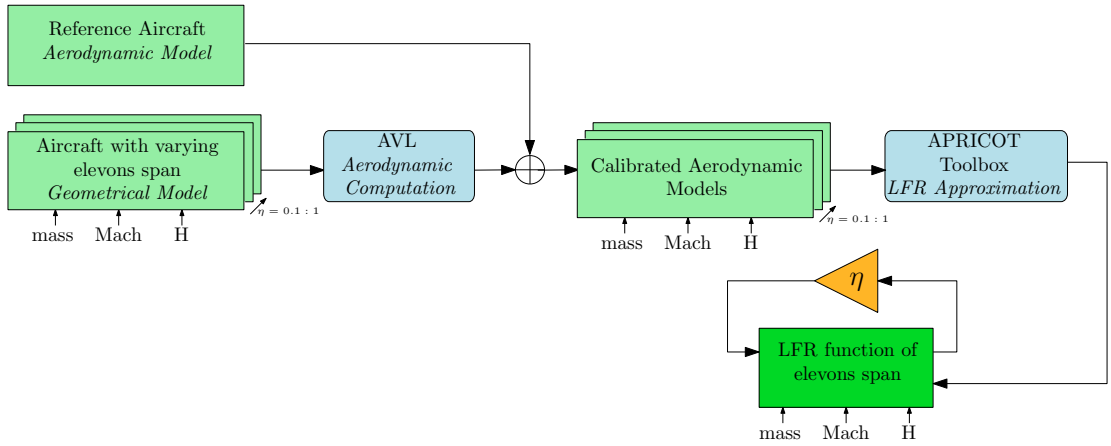

Fig. 3. Process for obtaining LFR approximation of state-space representations as a function of η parameter.

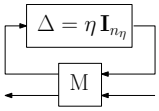

Fig. 4. Linear Fractional Representation of $B(\eta)$.

Representation (LFR) framework, because this representation is suited to the optimizer coming from the control community presented in section 4. Moreover efficient algorithms for approximating a set of numerical data as an LFR were developed by Onera Roos et al. (2014). An LFR is a model where all fixed dynamics are gathered in a single linear time-invariant plant M, whereas uncertainties or varying parameters are contained in a block-diagonal matrix Δ (see Figure 4). Polynomial and rational expressions are for instance easily convertible into LFR.

More precisely, the problem is that of finding an LFR approximating as closely as possible state-space representations computed for different values of η. Uncertainties are not considered in this study, so the Δ block is only composed of η parameter repeated n_η times. It was decided to restrict search for LFR approximations to polynomial approximations in order to keep the LFR order n_η as small as possible. From a physical perspective this can be justified by the fact that control surfaces efficiencies should vary smoothly with respect to their span. The least-squares routine `lsapprox` from APRICOT library on Matlab Roos et al. (2014) was used. A 5-th order polynomial approximation of the 8×11 $B(\eta)$ matrix leads to an LFR with $n_\eta = 20$. Maximum root-mean-square (RMS) is $9.36.10^{-3}$ and maximum local absolute error is $2.01.10^{-2}$. `lsapprox` instead of orthogonal least-squares `olsapprox` routine was used for it achieves higher accuracy.

4. INTEGRATED DESIGN AND CONTROL

In this section the integrated design and control problem of simultaneously minimizing elevons span parameter η while satisfying handling qualities and maneuverability constraints is developed.

4.1 Structure of Control Laws

As stated in section 2.2, longitudinal instability on this BWB requires a SAS to make it flyable. Moreover lateral control laws are also mandatory to enhance lateral handling qualities. Considering both these longitudinal and lateral / directional control laws is moreover necessary for a proper sizing of control surfaces. A main contribution of this paper is indeed to provide a methodology for *simultaneous* longitudinal, lateral and directional control laws synthesis of arbitrary structure, whereas this problem is usually treated by decoupling longitudinal from lateral / directional axes. Here a typical fly-by-wire FCS architecture is considered. Pilot provides inputs in terms of commanded load factor Nz_c, bank angle ϕ_c and sideslip β_c. Control law feedback features C^* and Y^* structure for longitudinal and lateral/directional control respectively, whose structure is provided in Favre (1994). More precisely:

- C^* structure is composed of load factor Nz and pitch rate q feedback, together with an integrator for zero steady-state tracking error and a direct feedthrough gain. Output of the law is an equivalent elevator order δm_{equi}.
- Y^* structure features lateral / directional state feedback, namely sideslip β, yaw rate r, bank angle ϕ and

roll rate p. An integrator is added to keep zero steady-state sideslip, as well as a bank angle order direct feedthrough gain. Outputs of this law are equivalent aileron and rudder order δl_{equi} and δn_{equi} respectively.

All the gains involved in the C^* and Y^* structured controllers are gathered in K as decision variables. A general overview of control law structure is visible on Figure 5. As already mentioned, control laws outputs are equivalent elevator, aileron and rudder orders, which are independent from control surfaces architecture. These equivalent orders are then converted into control surfaces deflections thanks to a control allocation module described in next section.

4.2 Control Allocation Model

Control allocation is the problem of converting equivalent orders, computed by the control law, into control orders when there are more effectors than axes to control. For a comprehensive survey of control allocation methods, please refer to the work by Johansen and Fossen (2013). In our study a control allocation module needs to be incorporated in order to convert equivalent elevator, aileron and rudder deflections $(\delta m_{equi}, \delta l_{equi}, \delta n_{equi})$ into actual control surfaces deflections $(\delta m_{i,i=1...10}, \delta n)$.

Mathematically, the control allocation problem is that of finding a deflections vector $\boldsymbol{u}$ satisfying:

$$\underbrace{\begin{bmatrix} Cm_{\delta m_1} & ... & Cm_{\delta m_{10}} & Cm_{\delta n} \\ Cl_{\delta m_1} & ... & Cl_{\delta m_{10}} & Cl_{\delta n} \\ Cn_{\delta m_1} & ... & Cn_{\delta n_{10}} & Cn_{\delta n} \end{bmatrix}}_{B_1(\eta)} \boldsymbol{u} = \begin{bmatrix} Cm_{\delta m_{equi}} \delta m_{equi} \\ Cl_{\delta l_{equi}} \delta l_{equi} \\ Cn_{\delta n_{equi}} \delta n_{equi} \end{bmatrix} \tag{6}$$

where $B_1(\eta)$ is the matrix of elevons gradients in pitch, roll and yaw respectively, which all depend from parameter η. $[Cm_{\delta m_{equi}}\ Cl_{\delta l_{equi}}\ Cn_{\delta n_{equi}}]^T$ is a vector of equivalent gradients as seen by the control law. These values may be set arbitrarily without loss of generality, we chose equivalent values of 1 on all axes. Then a classical solution of equation 6 is the Moore-Penrose pseudo-inverse:

$$\boldsymbol{u} = K_{alloc}(\eta) \begin{bmatrix} \delta m_{equi} \\ \delta l_{equi} \\ \delta n_{equi} \end{bmatrix} \tag{7}$$

$$\text{with } K_{alloc}(\eta) = B_1^T (B_1 B_1^T)^{-1} \tag{8}$$

As comprehensively discussed in section 4.3, our process features two steps. In the first step, three-axes gains are computed for a fixed η value; in this step the pseudo-inverse control allocation from equation (8) is used. During the second step, three-axes control law gains and η parameter are simultaneously optimized. In this step, K_{alloc} is no more fixed, but is a variable for the optimization. By doing this, the design space is widened, and a truly optimal strategy with respect to the imposed handling qualities constraints can be chosen by the optimizer.

More precisely, in order to limit the number of variables for the optimization, K_{alloc} is parameterized as follows:

$$K_{alloc} = \begin{bmatrix} K_{alloc}^{pitch} & K_{alloc}^{roll} & 0 \\ K_{alloc}^{pitch} & -K_{alloc}^{roll} & 0 \\ 0 & 0 & K_{alloc}^{yaw} \end{bmatrix} \tag{9}$$

This means we impose a symmetrical and anti-symmetrical deflection of the elevons for a pitch and roll order respectively, and a yaw order is allocated to the rudder only. By incorporating this physical knowledge of the control allocation structure, the number of variables within K_{alloc} is reduced from 33 to 11 variables.

4.3 Simultaneous Three-Axes Control Law Synthesis

Integrated design and control of the BWB presented in this paper follows a two-steps scheme:

(1) A first control laws synthesis computes gains for an arbitrarily fixed η value. The problem consists in minimizing the difference between a reference model and the closed-loop aircraft. The output of this step is the optimum value of the H_∞ criterion. This section is devoted to describing this first step.
(2) Output of step 1 is used to put a constraint on maximal value of the H_∞ criterion, in order to guarantee satisfactory closed-loop behavior while optimizing the elevons size η and control law gains. This step is described extensively in next section.

As stated previously, simultaneously optimizing control surfaces size η and control law gains requires setting a constraint – in the optimization sense – that ensures an adequate closed-loop behavior of the optimal solution. This constraint was set as a maximal admissible value of an H_∞ criterion, value which must be computed through a first synthesis. The H_∞ criterion and its optimal value computation are described now.

A three-channels model-reference tracking scheme was used. This scheme consists in minimizing the difference between a reference dynamics model and the closed-loop aircraft, from the H_∞ norm point of view. If the reference model is perfectly matched by the closed-loop in the whole frequency-domain, then the optimal H_∞ value is zero. However this is practically infeasible due to physical limitations, as a consequence the optimal value is always above zero.

Here model-reference tracking is written as minimizing the H_∞ norm of a three-input three-output transfer function between pilot inputs (Nz_c, ϕ_c, β_c) and outputs (z_1, z_2, z_3) the differences between reference dynamics outputs and actual closed-loop signals (Nz, ϕ, β). For a proper definition of signals please refer to Figure 5. In our case multi-channel transfer has several advantages over multiple single-input single-output (SISO) transfers. First off-diagonal terms are implicitly set to zero. Hence resulting control law will totally decouple all three axes, namely longitudinal from lateral / directional, but also lateral from directional – turns are performed with zero sideslip – and directional from lateral – "pedal" inputs imply no bank –. Couplings between all axes are explicitly taken into account by the control law, which a SISO approach would not. A single constraint on the H_∞ norm of this multi-channel transfer ensures an adequate closed-loop behavior

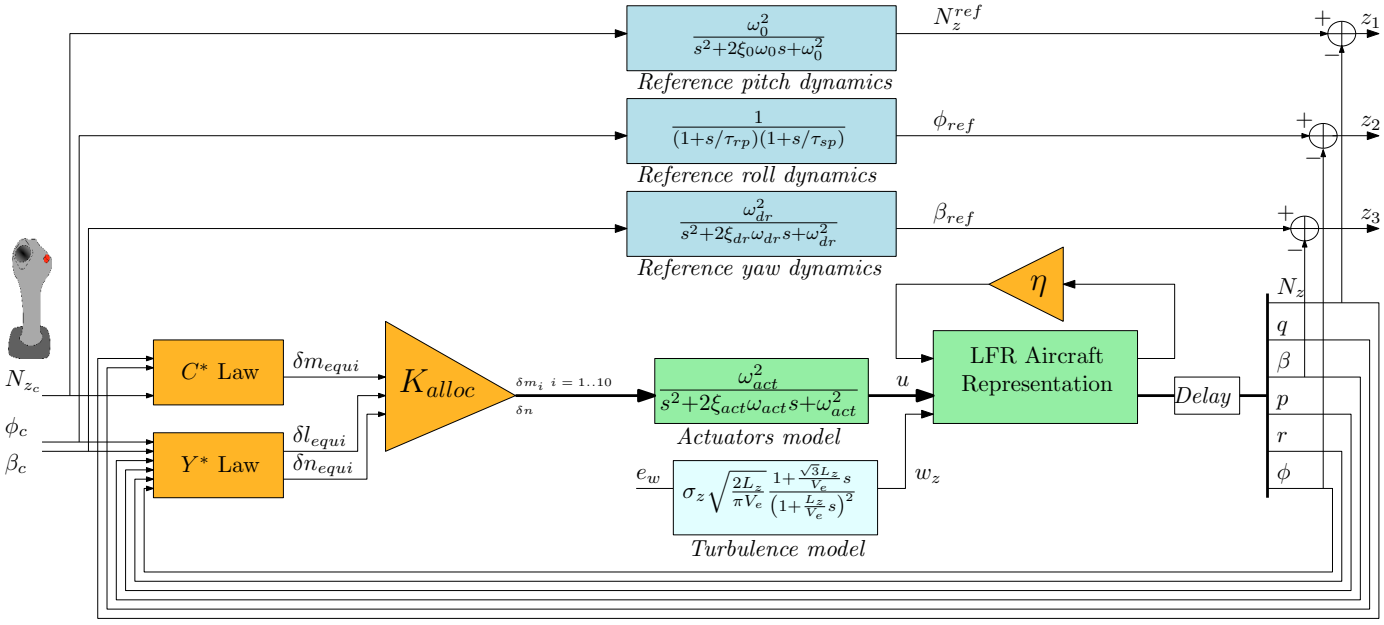

Fig. 5. Closed-loop representation for integrated design and control optimization.

on all three axes. An equivalent formulation with SISO transfers would require nine constraints.

In our study the closed-loop reference values are fixed and are given in table 1. The optimization problem for simultaneous three-axes control laws synthesis simply reads:

$$\min_K \left\| T_{(Nz_c,\phi_c,\beta_c)\to(z_1,z_2,z_3)}\left(P(\eta^{init}), K, K_{alloc}^{init}\right)\right\|_\infty = \hat{\gamma}_\infty$$
such that: (10)
$\forall p$, pole of $P(s)$:
$Re(p) \leq -\text{MinDecay}, Re(p) \leq -\text{MinDamping}.|p|;$
K internally stabilizes $P(\eta)$

K being a vector containing all control law gains defined in section 4.1. The additional constraints ensure that closed-loop poles have a damping of at least 0.5 (MinDamping), and a real part of at least 0.2 (MinDecay). Even though those constraints may seem redundant with the reference model tracking objective, it was found that it helps the optimizer to converge and to control indirectly the integral terms dynamics.

To solve this optimization problem, the `systune` routine Apkarian (2012) from Matlab Robust Control Toolbox was used. This routine allows tuning of fixed-order structured controllers, so it can handle physical parameters optimization combined with control gains computation. Couplings between control and design problem are therefore taken into account directly in a single optimization. Moreover it is well suited to mathematical particularities of the optimization problem in equation (10), namely the non-smooth behavior of the H_∞ norm. Optima found by the algorithm are only local, consequently several initializations should be performed in order to ensure the globality of the solution.

Parameter	ω_0	τ_{rp}	τ_{sp}	ω_{dr}
Value ($ad.s^{-1}$)	1	1.6	1.9	0.4

Table 1. Reference model ($\xi_0 = \xi_{dr} = 0.7$).

4.4 Definition of the Optimization Problem

Once the optimum $\hat{\gamma}_\infty$ of the H_∞ criterion is computed, it is used as a constraint on the H_∞ norm of the multi-channel transfer for the combined optimization problem. More precisely the integrated design and control problem of this study is that of finding a minimal η such that:

- Deflections and deflection rates in response to maneuvers do not exceed prescribed limits.
- Closed-loop behavior is optimal.

The latter point is solved by ensuring that the H_∞ norm of the multi-channel transfer $\|T_{(Nz_c,\phi_c,\beta_c)\to(z_1,z_2,z_3)}(\eta)\|_\infty$ is kept under its optimal value $\hat{\gamma}_\infty$ whatever η. Once the optimum value $\hat{\gamma}_\infty$ for a fixed η is known from the optimization described in section 4.3, the optimization problem of finding the best possible closed-loop behavior translates into a single constraint satisfaction problem. This elegant formulation allows minimizing an other objective, – η in our case – while designing appropriate control law gains to ensure a satisfactory closed-loop behavior on all axes.

Constraints on maneuverability are cast as constraints on the H_∞ norm of adequate transfer functions, similarly to the work of Niewoehner and Kaminer (1996). Therefore these constraints are root-mean-square (RMS) and not temporal. Following constraints are ensured:

- Maximum deflections and deflections rate in response to a pilot pull-up. This is ensured through constraint on following H_∞ norms: $\|\frac{1}{\Delta\delta m_i^{max}} T_{Nz_c\to u}\Delta N z_c^{max}\|_\infty \leq 1$ and $\|\frac{1}{\dot{\delta m}_i^{max}} T_{Nz_c\to \dot{u}}\Delta N z_c^{max}\|_\infty \leq 1$ respectively, with $\Delta\delta m_i^{max} = \delta m_i^{max} - \delta m_e$.
- Maximum deflections and deflections rate in response to severe longitudinal turbulence. This is ensured through constraint on following H_∞ norms: $\|\frac{2}{\Delta\delta m_i^{max}} T_{e_w\to u}\|_\infty \leq 1$ and $\|\frac{2}{\dot{\delta m}_i^{max}} T_{e_w\to \dot{u}}\|_\infty \leq 1$ respectively.

- Maximum deflections and deflections rate in response to ϕ^{max} bank angle order. This is ensured through constraint on following H_∞ norms: $\|\frac{1}{\Delta\delta m_i^{max}} T_{\phi_c \to u} \phi^{max}\|_\infty \leq 1$ and $\|\frac{1}{\dot{\delta m}_i^{max}} T_{\phi_c \to \dot{u}} \phi^{max}\|_\infty \leq 1$ respectively.

Chosen values for the sizing are:
$\delta m^{max} = 25°$, $\dot{\delta m}^{max} = 60°/s$, $\Delta N z_c^{max} = 1.5g$, $\phi_c^{max} = 45°$.

The combined optimization problem is finally summarized in Tab. 2 and is extensively described in Denieul (2016).

5. RESULTS

In this section the results of the integrated design and control process are analyzed.

5.1 Integrated Design and Control on a Single Flight Point

Integrated design and control with tunable allocation applied to the flight point $M.35$, $H = 3300ft$, $m = 300T$ gives following results:

$$\eta^{opt} = 0.3885 \tag{11}$$
$$gBest = 0.9998 \tag{12}$$

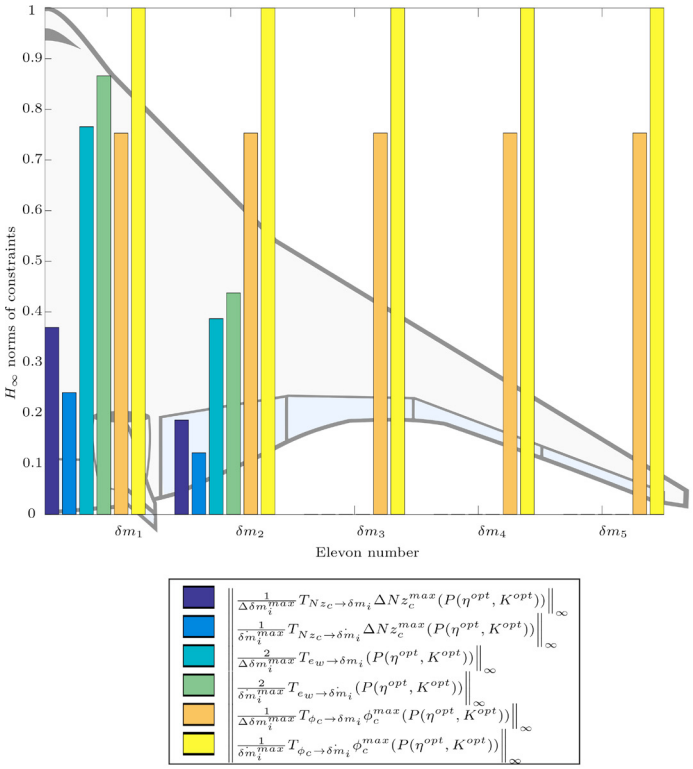

Fig. 6. Bar diagram of normalized constraints values after optimization with tunable allocation, $\eta^{opt} = 0.3885$.

A 61% decrease of the control surfaces span is achieved compared to the initial layout, while still satisfying all handling qualities constraints – i.e. $gBest < 1$. More precisely Figure 6, gathering all handling qualities constraints at the optimum, indicates that on this flight point the roll constraint is limiting. As a consequence, the optimal allocation is to distribute equally among all elevons the roll order, hence all roll criteria are equally saturated. Pitch being not limiting on this flight point, only two pairs of elevons are used for pitch control. This behavior is confirmed by looking at the optimized allocation matrix:

$$K_{alloc}^{opt} = \begin{bmatrix} 0.023 & 0.3811 & 0 \\ 0.0116 & 0.3811 & 0 \\ 0.000 & 0.3811 & 0 \\ 0.000 & 0.3811 & 0 \\ 0.000 & 0.3811 & 0 \\ 0.023 & -0.3811 & 0 \\ 0.0116 & -0.3811 & 0 \\ 0.000 & -0.3811 & 0 \\ 0.000 & -0.3811 & 0 \\ 0.000 & -0.3811 & 0 \\ 0.000 & 0.000 & 0.006 \end{bmatrix} \tag{13}$$

6. CONCLUSION

A new method for sizing control surfaces of an unstable blended wing-body using closed-loop handling qualities criteria was presented. This method consists in simultaneously optimizing the longitudinal and lateral control laws, as well as a control allocation module, while minimizing the control surface areas under handling qualities constraints. From a sizing perspective, we have shown that the studied Airbus BWB configuration can adequately be controlled on all three axes with only 60% of the initial control surfaces span, with normal laws and full control authority, with reasonable hypotheses on the actuators, sensors and delays chain. Future work will extend such a procedure to the full flight envelope. Temporal criteria instead of frequency – root-mean-square – criteria will be also investigated. Finally alternative optimizers could be considered for solving this coupled problem; simulation-based routines such as genetic algorithms could be worth examining.

REFERENCES

Alazard, D., Loquen, T., de Plinval, H., and Cumer, C. (2013). Avionics/Control co-design for large flexible space structures. In *AIAA Guidance, Navigation, and Control (GNC) Conference*, Guidance, Navigation, and Control and Co-located Conferences. American Institute of Aeronautics and Astronautics.

Apkarian, P. (2012). Tuning Controllers Against Multiple Design Requirements. In *System Theory, Control and Computing (ICSTCC), 2012 16th International Conference on*, 1–6. IEEE.

Bolsunovsky, A., Buzoverya, N., Gurevich, B., Denisov, V., Dunaevsky, A., Shkadov, L., Sonin, O., Udzhuhu, A., and Zhurihin, J. (2001). Flying wing—problems and decisions. *Aircraft Design*, 4(4), 193–219.

Denieul, Y. (2016). *Preliminary Design of Control Surfaces and Laws for Unconventional Aircraft Configurations*. Mémoire de thèse, ISAE-Supaéro, Toulouse, France.

Denieul, Y., Alazard, D., Bordeneuve, J., Toussaint, C., and Taquin, G. (2015a). Interactions of Aircraft Design and Control: Actuators Sizing and Optimization for an Unstable Blended Wing-Body. In *AIAA Atmospheric Flight Mechanics Conference*, AIAA Aviation. American Institute of Aeronautics and Astronautics, Dallas, TX.

	Function / Variable	Description	Quantity
minimize	η	Outer elevons total span	
with respect to	K	Control law gains	16
	K_{alloc}	Control allocation matrix	11
	η	Outer elevons total span	1
subject to	$\|\frac{1}{\Delta\delta m_i^{max}} T_{Nz_c \to u} \Delta\alpha \frac{V_e}{g} z_\alpha\|_\infty \leq 1$	Maximum deflection in response to longitudinal order.	5
	$\|\frac{1}{\dot{\delta m}_i^{max}} T_{Nz_c \to \dot{u}} \Delta\alpha \frac{V_e}{g} z_\alpha\|_\infty \leq 1$	Maximum deflection rate in response to longitudinal order.	5
	$\|\frac{2}{\Delta\delta m_i^{max}} T_{e_w \to u}\|_\infty \leq 1$	Maximum deflection in response to longitudinal turbulence	5
	$\|\frac{2}{\dot{\delta m}_i^{max}} T_{e_w \to \dot{u}}\|_\infty \leq 1$	Maximum deflection rate in response to longitudinal turbulence	5
	$\|\frac{1}{\Delta\delta m_i^{max}} T_{\phi_c \to u} \phi^{max}\|_\infty \leq 1$	Maximum deflection in response to bank order.	5
	$\|\frac{1}{\dot{\delta m}_i^{max}} T_{\phi_c \to \dot{u}} \phi^{max}\|_\infty \leq 1$	Maximum deflection rate in response to bank order.	5
	$\|T_{(Nz_c, \phi_c, \beta_c) \to (z_1, z_2, z_3)} \cdot \frac{1}{\tilde{\gamma}_\infty}\|_\infty \leq 1$	Optimal closed-loop performance.	1
	$\forall p, p$ pole of $P(s)$: $Re(p) \leq -\text{MinDecay}, Re(p) \leq -\text{MinDamping}.\|p\|$ K internally stabilizes $P(\eta)$	Closed-loop poles location.	1

Table 2. Integrated design and control optimization problem.

Denieul, Y., Bordeneuve, J., Alazard, D., Toussaint, C., and Taquin, G. (2015b). Integrated Design and Control of a Flying Wing Using Nonsmooth Optimization Techniques. In J. Bordeneuve, A. Drouin, and C. Roos (eds.), *Advances in Aerospace Guidance, Navigation and Control*, 475–489. Springer International Publishing.

Drela, M. and Youngren, H. (2006). AVL Aerodynamic Analysis, Trim Calculation, Dynamic Stability Analysis, Aircraft Configuration Development.

Fathy, H., Reyer, J., Papalambros, P., and Ulsov, A. (2001). On the Coupling Between the Plant and Controller Optimization Problems. In *American Control Conference, 2001. Proceedings of the*, volume 3, 1864–1869 vol.3.

Favre, C. (1994). Fly-by-wire for commercial aircraft: the Airbus experience. *International Journal of Control*, 59(1), 139–157.

Garmendia, D.C., Chakraborty, I., Trawick, D.R., and Mavris, D.N. (2014). Assessment of Electrically Actuated Redundant Control Surface Layouts for a Hybrid Wing Body Concept. In *14th AIAA Aviation Technology, Integration, and Operations Conference*, AIAA Aviation. American Institute of Aeronautics and Astronautics.

Johansen, T.A. and Fossen, T.I. (2013). Control allocation- a survey. *Automatica*, 49(5), 1087–1103.

Lhachemi, H., Saussie, D., and Zhu, G. (2015). A structured -based optimization approach for integrated plant and self-scheduled flight control system design. *Aerospace Science and Technology*, 45(0), 30–38.

Liebeck, R.H. (2004). Design of the Blended Wing Body Subsonic Transport. *Journal of Aircraft*, 41(1), 10–25.

Martínez-Val, R. and Pérez, E. (2005). Medium Size Flying Wings. von Karman Institute for Fluid Dynamics.

Meheut, M., Arntz, A., and Carrier, G. (2012). Aerodynamic Shape Optimizations of a Blended Wing Body Configuration for Several Wing Planforms. In *AIAA*, volume 10, 3122. American Institute of Aeronautics and Astronautics, New Orleans, Louisiana.

Niewoehner, R.J. and Kaminer, I. (1996). Integrated Aircraft-Controller Design using Linear Matrix Inequalities. *Journal of Guidance, Control, and Dynamics*, 19(2), 445–452.

Perez, R., Liu, H., and Behdinan, K. (2006). A Multidisciplinary Optimization Framework for Control-Configuration Integration in Aircraft Conceptual Design. *Journal of Aircraft*, 43(6), 1937–1948.

Qin, N., Vavalle, A., Le Moigne, A., Laban, M., Hackett, K., and Weinerfelt, P. (2004). Aerodynamic considerations of blended wing body aircraft. *Progress in Aerospace Sciences*, 40(6), 321–343.

Ricardez-Sandoval, L., Budman, H., and Douglas, P. (2009). Simultaneous design and control of chemical processes with application to the Tennessee Eastman process. *Journal of Process Control*, 19(8), 1377–1391.

Roman, D., Allen, J., and Liebeck, R. (2000). Aerodynamic Design Challenges of the Blended-Wing-Body Subsonic Transport. In *18th Applied Aerodynamics Conference*. AIAA.

Roos, C., Hardier, G., and Biannic, J.M. (2014). Polynomial and rational approximation with the APRICOT Library of the SMAC toolbox. In *Control Applications (CCA), 2014 IEEE Conference on*, 1473–1478.

Roskam, J. (1985). *Airplane Design Part VI: Preliminary Calculation of Aerodynamic, Thrust and Power Characteristics*. DARcorporation, Kansas.

Saucez, M. and Boiffier, J.L. (2012). Optimization of Engine Failure on a Flying Wing Configuration. In *AIAA Atmospheric Flight Mechanics Conference*, Guidance, Navigation, and Control and Co-located Conferences. AIAA, Minneapolis, Minnesota.

Silvestre, C., Pascoal, A., Kaminer, I., and Healey, A. (1998). Plant-Controller Optimization with Applications to Integrated Surface Sizing and Feedback Controller Design for Autonomous Underwater Vehicles (AUVs). In *American Control Conference*, volume 3, 1640–1644.

Standard, M. (1990). Flying Qualities of Piloted Aircraft. Technical report, MIL-STD-1797A, Department of Defense.